Middle Black Sea Journal of Health Science / Mid Blac Sea J Health Sci
August 2025; 11(3): 190-211

ORGINAL ARTICLE **DOI:** 10.19127/mbsjohs.1603923

Ocimum basilicum-Assisted Gold Nanoparticle Formation: Structural Features and Antimicrobial Performance

Muhammed Said Özonay[1(ID)], Cumali Keskin[2(ID)], Ayşe Baran[3(ID)], Özgür Topgider[4(ID)], Şeyma Asyalı[4(ID)]

[1]Mardin Artuklu University, Vocational School of Organized Industrial Zone, Department of Electronics and Automation, Mardin, Türkiye
[2]Mardin Artuklu University, Vocational School of Health Science, Department of Medical Services and Techniques, Mardin, Türkiye
[3]Mardin Artuklu University, Kızıltepe Faculty of Agricultural Sciences and Technologies, Department of Field Crops, Mardin, Türkiye
[4]Mardin Artuklu University, Graduate Education Institute, Department of Biology, Mardin, Türkiye

Received: 06 May 2025, Accepted: 30 July 2025, Published online: 30 August 2025

Abstract

Objective: Plant-based biosynthesis of gold nanoparticles (AuNPs) can reduce the biological consequences of NPs released into the environment by replacing toxic substances. The Lamiaceae family includes the perennial herb *Ocimum basilicum* (OB), which is typically found in temperate climates. This study aimed to synthesize biogenic metallic nanoparticles ecologically to provide agricultural, medical, and pharmacological options from OB leaf aqueous extract.

Method: Tetrachloroauric acid ($HAuCl_4.3H_2O$) solution and OB extract were the chemicals, stabilizers, or surfactants used in the biological synthesis process to create gold nanoparticles (OB-AuNPs). Data from UV-Vis, SEM-EDX, XRD, FT-IR, TGA-DTA, AFM, and zeta potential were used to characterize the produced AuNPs. The minimum inhibitory concentration (MIC) method was used to test the antimicrobial activity.

Results: UV-Vis data revealed that the produced gold nanoparticles produced a notable plasmon resonance at around 532 nm. SEM-EDX examination verified that the synthesized nanomaterials had a spherical crystal structure. The reduction of Au^{+3} ions using the OB extract resulted in the production of crystalline AuNPs, as demonstrated by the high-resolution and robust XRD pattern. Analysis of XRD and SEM-EDX data revealed that gold, oxygen, and carbon made up the majority of OB-AuNPs' element content. The surface charges of AuNPs were determined to be (−) 17 mV.

Conclusion: The negative zeta potential indicates good stability of the nanoparticles in suspension, suggesting that they are less likely to aggregate over time. It was found that, in comparison to conventional antibiotics, OB-AuNPs produced utilizing an extract from the leaves of the OB had more potent inhibitory activity on the growth of yeast and pathogenic gram bacteria. Overall, these findings support the potential application of AuNPs in various fields, including biomedical and environmental technologies.

Keyword: *Ocimum basilicum* (Basil extract), antimicrobial activity, characterization, plant-mediated synthesis, gold nanoparticles (AuNPs)

Suggested Citation Ozonay MS, Keskin C, Baran A, Topgider O, Asyali S. Ocimum basilicum-Assisted Gold Nanoparticle Formation: Structural Features and Antimicrobial Performance. Mid Blac Sea Journal of Health Sci, 2025;11(3):190-211.

Address for correspondence/reprints:

Cumali Keskin

Telephone number: +90 (532) 741 39 89

E-mail: cumalikeskin@artuklu.edu.tr

INTRODUCTION

Nanotechnology has emerged as a transformative tool across diverse fields, particularly in medicine, where it enables targeted drug delivery, advanced diagnostics, and novel antimicrobial therapies. In recent years, plant-mediated synthesis of nanoparticles has gained prominence due to its eco-friendly and biocompatible nature, positioning it as a promising strategy in biomedical nanotechnology (1). Drugs, inanimate materials inserted into live tissues, and blocking veins can all be accomplished with the use of nanotechnology-developed products (2). These advancements enhance the efficacy of medical treatments and pave the way for personalized medicine, where therapies can be tailored to individual genetic profiles. As research continues to evolve, the potential applications of nanotechnology in healthcare promise to revolutionize the way we approach disease management and tissue regeneration (3).

Also, nanotechnology is favored for producing nanoparticles using quick, inexpensive, and environmentally acceptable "green synthesis" techniques that address various health-related issues (4). The two most common methods for creating nanoparticles are top-down and bottom-up. The "top-down" technique reduces the size of nanostructured materials by abrading the larger, macro-sized material toward the nanoscale. The "bottom-up" method joins particles to create larger ones. Both approaches have their unique advantages and applications, depending on the desired properties and functionalities of the final product. As research progresses, the integration of these methods could lead to innovative solutions across multiple fields, including medicine, electronics, and environmental science (5).

The scientific community has recently shown considerable interest in noble metal nanoparticles (MNPs), particularly gold (AuNP) and silver (AgNP), due to their remarkable properties such as strong photo-electrochemical activity, chemical stability, biocompatibility, and exceptional capabilities in catalyzing chemical reactions and combating pathogens, along with their ease of synthesis. These characteristics render MNPs highly suitable for a broad array of applications, including drug delivery, biosensing, and

environmental remediation. As research continues to investigate their potential, the integration of MNPs into various technologies could lead to significant advancements in fields like medicine and environmental science (5,6).

Applications for metallic nanoparticles, particularly gold nanoparticles (AuNPs), are numerous in the field of biomedicine. Additionally, differently sized and shaped gold nanostructures have been found to impact cell viability (7). Gold nanoparticles will range in size from 2 to 370 nm. Hexahedral, octahedral, cubic, prismatic, plate, wire, spherical, trihedral, and tetrahedral shapes are among them. The terms nanosphere, nanorod, nanocube, nanowire, and nanoprism are being used to describe them (8). The surface resistance features of gold nanoparticles make them useful for a wide range of applications, including cell targeting, nanoimaging, and disease diagnostics in photoelectronics. Additionally, biomolecular investigations that detect drug and gene release favor them. Gold nanoparticles are among the best agents for treatment because they can transport large drug loads and readily reach target bio-cells (9). Gold nanoparticles, which are widely employed in processes like biolabeling and photothermal microscopy, have emerged as a promising option for imaging and biosensor applications because of their high electron density (10). They are known to have less antibacterial activity than silver, but their ease of synthesis has made them useful for applications in fields including biomedical imaging and photothermal health (11).

Studies have been done on making gold nanoparticles (AuNPs) using natural sources like plants (12), fungi (13), algae (14), bacteria (15), and seaweeds (16) through eco-friendly methods. The main reasons for researching this area are the large quantities of AuNPs produced from different parts of plants like leaves, fruits, roots, and flowers, their improved stability, and the easy and affordable methods used to make them. Bioactive substances like alcohols, flavonoids, and phenolic compounds from plants help turn Au^{3+} ions in water into AuNPs by producing Au^{0} (10).

Potential uses for these nanoparticles include bioremediation, antiviral, antibacterial, antioxidant, cytotoxic, antitumor, anti-inflammatory, and antidiabetic (17). Microbial infections have grown more resistant to even the most effective therapies recently. The healthcare system has been strained as a result of the rise in mortality and morbidity worldwide. Concerns have arisen about the use of antibiotics and the research process for developing new ones, underscoring the urgent need to halt this threat. More people are looking for different ways to fight antibiotic resistance and create new medications (18).

Biogenic nanoparticles derived from plant sources can serve as carriers and enhance cellular penetration for many applications.

Nanoparticles possess considerable advantages owing to their distinct surface area and favorable conductivity. Biogenic nanoparticles have significantly contributed to the advancement of novel techniques in biomedicine and pharmacology (19). These advancements encompass the creation of intelligent pharmaceutical substances alongside diagnostic and therapeutic methodologies (20). This study primarily aims to synthesize metallic gold nanoparticles utilizing an aqueous leaf extract of OB. The utilization of extracts derived from O.B. leaves, facilitated by their abundance, provides a straightforward and cost-effective approach for the synthesis of metallic nanoparticles.

O.B., which grows in tropical and temperate climates, is recognized in scientific circles as having Indian origin. Purple basil is an herbaceous plant that grows every year. Africa, America, and Asia are all naturally home to the *Ocimum* genus, and there are more than 35 species of basil. Depending on the linguistic and dialectal structures of the three regions of the world, they have different names. It is referred to as reihan in Turkey and the surrounding area and rehan in Arabic and Persian, respectively (21, 22). It is referred to as Albahaca in Spanish and *Basilic basilicum* in French and German. In Turkey, it is commonly referred to as basil. Badrooj, Hebak, or Rihan are further regional names. There are more than 65 species worldwide, and it is said to grow naturally in hot and temperate climates in Africa, Asia, and Central America (23). The morphology and chemical composition of *O. basilicum* vary greatly (24). The leaves and blossoms of basil (*O. basilicum*) and basil (*O. minimum*) are the most economically valuable portions. This research used an aqueous extract of the aboveground portions of the OB plant to examine the biosynthesis, synthesis, characterization, and antibacterial qualities of gold nanoparticles. The study aimed to highlight the potential applications of these gold nanoparticles in various fields, particularly in medicine and agriculture. By investigating their antibacterial properties, the research sought to establish a foundation for developing new antimicrobial agents derived from natural sources.

METHODS

Plant Materials and Reagents

The leaves of OB used in this study were obtained from the local market in Mardin in May. Dr. Cumali Keskin from Mardin Artuklu University confirmed the taxonomic identity of the plant sample. The plant samples were stored in the herbarium of the same institution (herbarium voucher number MAU: 2023-05). Tetrachloroauric acid (HAuCl4.3H2O, purity 99.99 %; Alfa Aesar) in solid form was used in the synthesis stage. The McFarland standard (0.5), Mueller Hinton medium, the RPMI feed medium, and standard antibiotics (fluconazole, vancomycin, and colistin) were commercially

purchased from Sigma Aldrich. The microorganisms used in the study were selected from the strains in the American Cell Culture Collection (ATCC) in the inventory of Mardin Artuklu University Microbiology Research Laboratory.

Preparation of Plant Extract

Distilled water was utilized to completely wash the OB leaves used in the experiment to get rid of any leftover residue. They were dried at room temperature and powdered on sterile blotting paper. After 50 g of the powdered samples were taken and boiled for 20 minutes at 85ºC with 750 mL of distilled water, the resulting aqueous extract was allowed to cool to room temperature (25ºC). Following that, Whatman filter paper was used to filter the coarse plant pieces. To be employed in the manufacture of gold nanoparticles, the resulting aqueous extract was kept at +4 °C.

Green Synthesis of OB-AuNPs

The solid form of tetra chloroauric acid ($HAuCl_4.3H_2O$) was used to prepare an aqueous gold solution with a concentration of 5 mM for the biosynthesis of AuNPs. At room temperature, 75 milliliters of aqueous extract of OB leaf and 100 milliliters of a solution of 5 mM $HAuCl_4.3H_2O$ were combined and allowed to react. 30 minutes into the reaction, Au^{3+} ions were reduced to Au^0, and the solution lost its transparency and turned dark red. After seeing the color change, the solution that was formed was centrifuged for twenty minutes at a speed of 6000 rpm, and the solid component was separated. Multiple washes with distilled water were performed on the solid phase that had accumulated at the bottom. OB-AuNPs that had been synthesized were allowed to dry in an oven at a temperature of 50 ºC for 72 hours. In an agate mortar, the solid component was then ground into a powder.

Figure 1. A. Fresh leaves of OB. B. Dried leaves. C. $HAuCl_4.3H_2O$ solution (Yellow). D. OB aqueous extract (Red). E. Biosynthesized OB-AuNPs solution (Dark red)

Characterization of Biogenic OB-Au NPs

A Shimadzu UV-1601 ultraviolet-visible spectrometer was used to identify the surface plasmon resonance (SPR) peaks of the biosynthesized OB-AuNPs. The shape and distribution of elements in OB-AuNPs were studied using a scanning electron microscope with energy-dispersive X-ray capabilities and

transmission electron microscopy. The surface charge and stability of OB-AuNPs in liquid were measured using a zeta potential and zeta-sizer device (Malvern). Differential thermal analysis (DTA) and thermogravimetric analysis (TGA) were used to check how stable OB-AuNPs are when heated and to measure any weight loss. The crystalline structure of OB-AuNPs was determined using XRD equipment (X-ray diffractometer RadB-DMAX 11). The topological characteristics of OB-AuNPs were analyzed utilizing Atomic Force Microscopy (AFM). FT-IR spectroscopy (650 cm^{-1} to 4000 cm^{-1}; Perkin Elmer One, USA) was used to study the functional groups in the plant extract and how they changed after the process was finished. This comprehensive approach allowed for a detailed understanding of the chemical transformations that occurred during the synthesis of OB-AuNPs. Furthermore, the results obtained from these analyses provided valuable insights into the stability and efficacy of the nanoparticles for potential applications in various fields, including medicine and environmental science.

Evaluation of the Antimicrobial Properties of Au Nanoparticles

OB-AuNPs, $HAuCl_4.3H_2O$ solution, and commercial antibiotics (fluconazole, vancomycin, and colistin) were tested for their ability to inhibit the growth of pathogenic microorganisms, including *Candida albicans* (*C. albicans*) yeast, *Escherichia coli* (*E. coli*; ATCC 25922) bacterial strains, and *Staphylococcus aureus* (*S. aureus*; ATCC 29213). They were plated on solid plates using nutrient agar solid medium for Gram-positive and Gram-negative bacteria and sabouraud dextrose agar medium for yeast. The solid medium plates' microorganisms were used to create solutions that met the McFarland standard 0.5 turbidity threshold (1.5×10^8 united colonies (cfu/mL). *C. albicans* yeast was cultured in Roswell Park Memorial Institute (RPMI) broth, while bacteria were cultured in Müller Hinton broth. For the microdilution procedure, 96-well microplates were utilized. The microdilution-applied microplates were incubated for an entire night at 37 °C. The lowest inhibitory concentrations and the wells in which growth took place were then calculated (25).

RESULTS

An aqueous extract that was generated from the leaves of OB was used in this publication to describe the results of research that investigated the biogenesis of gold nanoparticles. The selection of OB leaf for the present experiment was based on the fact that it is known to contain flavonoids and phenolic chemicals, both of which are known to contribute to the antibacterial activities of the leaf. The initially yellow $HAuCl_4$ solution turns purple, red, or violet as gold nanoparticles form. The phenolic compounds, flavonoids, terpenoids, ascorbic acid (vitamin C), sugars, and other reducing

agents found in plant extracts convert Au^{3+} ions (gold ions) to elemental gold (Au^0) when $HAuCl_4 \cdot 3H_2O$ (Gold (III) Chloride Trihydrate) combines with the plant aqueous extracts. The study aimed to explore the potential of these compounds in facilitating the reduction of gold ions into nanoparticles. By utilizing the extract, we were able to observe the formation of nanoparticles and analyze their size and morphology through various characterization techniques.

Characterization

UV-Vis Spectrophotometry Results

A spectrophotometer is used to test a solution's transmittance. Spectrophotometers assess transmittance or absorbance in relation to wavelength by altering it. They are preferred because of their excellent sensitivity, speed, applicability, and repeatability. Determining the structures of pure chemicals in food, determining if a functional group is present, and identifying the position of a functional group in a compound are all done via qualitative analysis. The occurrence of a surface plasmon resonance (SPR) peak at ~520-550 nm confirms the presence of gold nanoparticles (26). A maximum absorbance band was observed at 532.59 nm, confirming Au NPs' formation (Figure 2). The published results from the previous research were comparable to this set of findings. These similarities suggest a consistency in the results across different studies, reinforcing the validity of the conclusions drawn. Furthermore, the alignment of these findings may indicate a broader trend within the field that warrants further exploration (27).

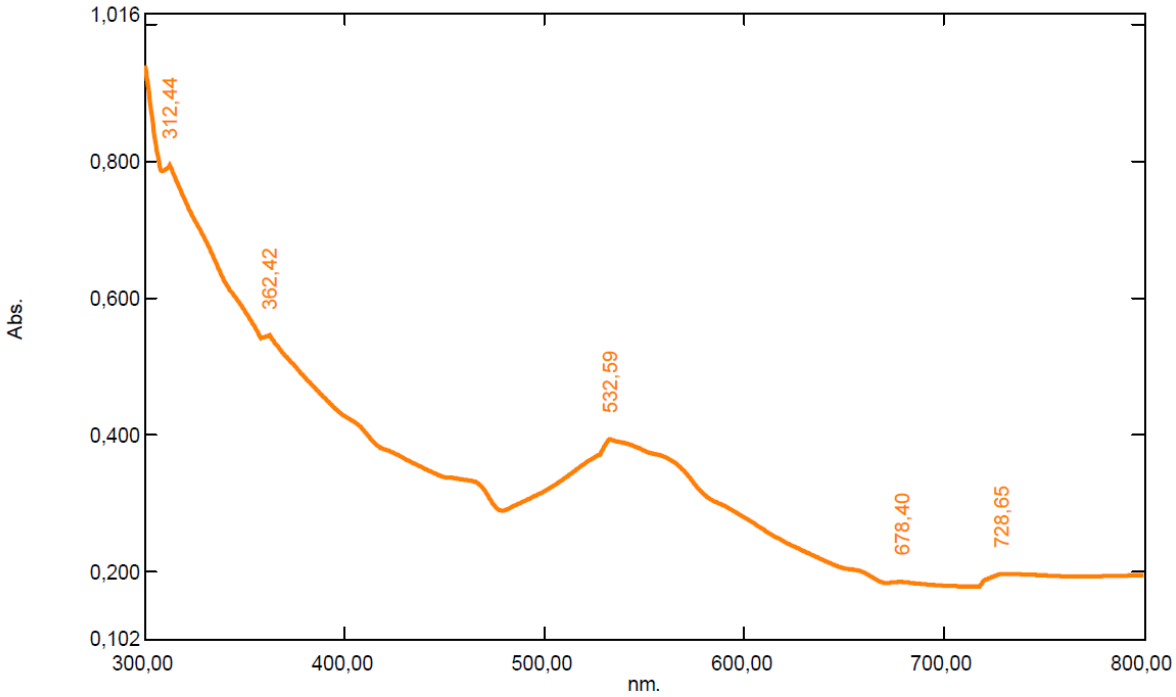

Figure 2. Ultraviolet-Visible absorption spectra of OB-AuNPs

FTIR Spectrum Data Analysis

The analysis performed with the FT-IR device in the range of 500–4000 cm^{-1} examined the presence of functional groups in the structure of the plant extract and the change of functional groups that play a role in the reduction at the end of the reaction. FT-IR spectroscopy is critical in investigating the chemical composition of chemical compounds. Here, it is used to characterize the plant extract and the nanoparticles synthesized from it. The FT-IR spectrum provides information about which functional groups the reaction took place on by comparing the extract from OB leaves (Figure 3a) and the synthesized OB-AuNPs (Figure 3b). This comparison allows researchers to identify specific peaks corresponding to various functional groups, indicating potential interactions during the synthesis process. Also, changes in these peaks can provide information about how the plant extract connects with the nanoparticles, helping us better understand the chemical changes that take place.

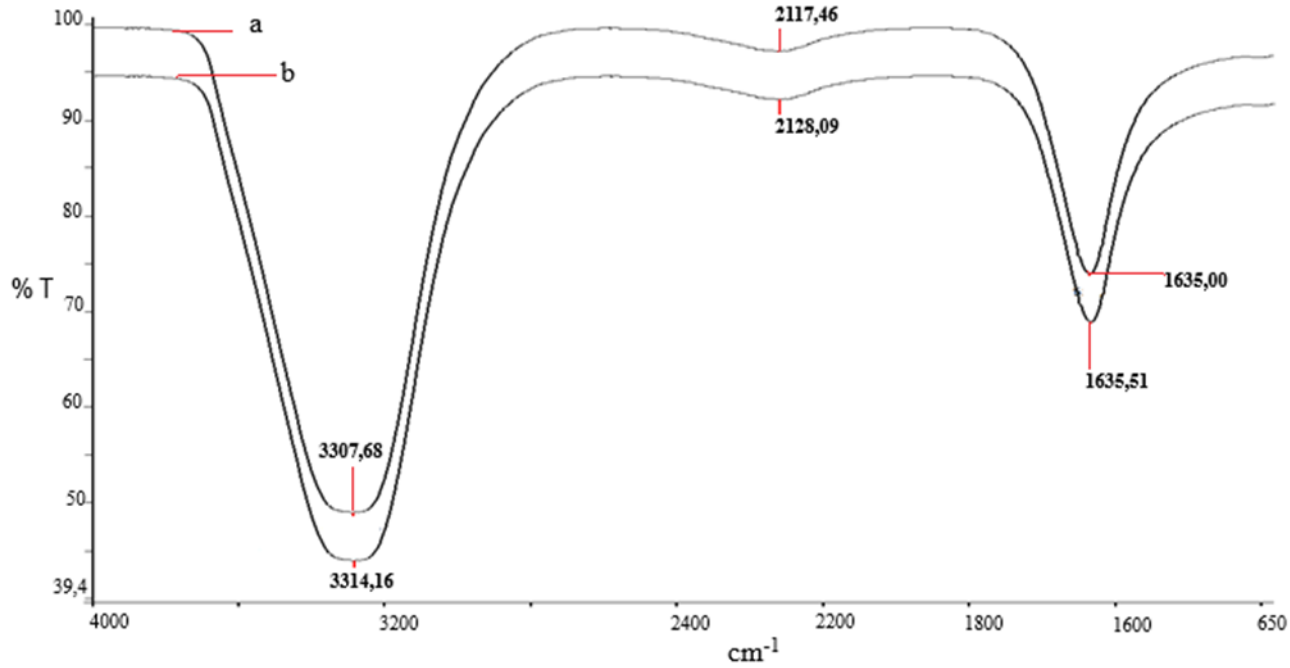

Figure 3. a. OB aqueous plant extract FT-IR spectrum b. OB-AuNPs FT-IR

XRD Analysis Data of OB-Au NPs

The crystal structures of gold nanoparticles were examined using a RadBDMAX II computer-controlled X-ray diffractometer within the region of $0° \leq 2\theta \geq 80°$. The crystal dimensions of gold nanoparticles were determined utilizing the Debye-Scherrer equation (25).

$$D = K\lambda/(\beta \cos(\theta)) \quad (1)$$

In the equation, D represents the crystal diameter of the particle (nm); K is 0.90; λ denotes the wavelength (1.54 Å); β signifies the breadth of the greatest peak at half height (rad.);

and θ indicates the Bragg angle degrees. The crystal structure (JCPDS No 04-0784) and purity of gold nanoparticles were verified using X-ray diffraction analysis. Figure 4 illustrates the powder XRD patterns of nano-crystalline AuNPs.

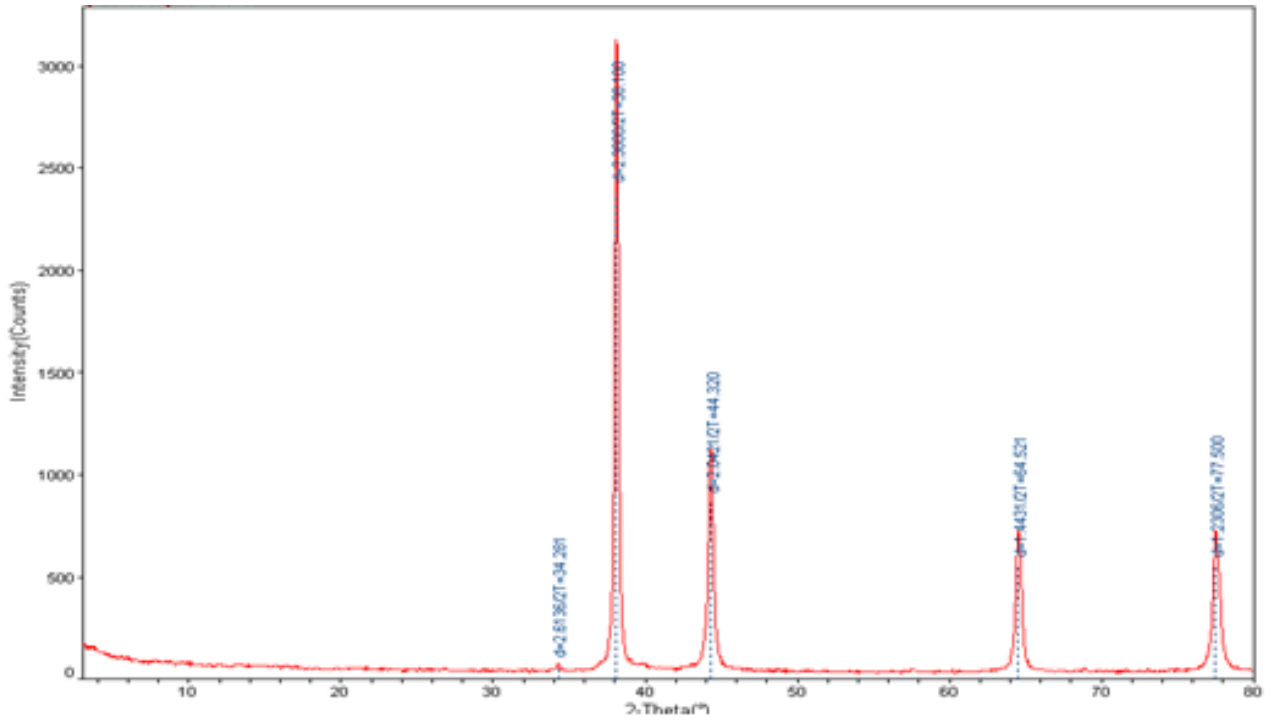

Figure 4. XRD pattern of biogenic OB-AuNPs

SEM-EDX and TEM Analysis of Green-Synthesized AuNPs

SEM and TEM image analyses were performed to determine the surface morphology and particle average size of AuNPs (Figures 5 and 6a,b). The images obtained from these analyses confirmed the existence of nano-sized AuNPs obtained using biological material. The angle of incidence of the electron beam on the surface, or the surface topography, determines how many secondary electrons are released from various regions of the sample by atoms excited by the electron beam in scanning electron microscopy. Analyses of composition and topography were carried out as needed. SEM, or scanning electron microscopy, was used to determine the size and shape of the gold nanoparticles. The creation of pure gold or gold oxide particles of AuNPs in the basic composition was verified using SEM-energy dispersive X-ray spectroscopy (SEM-EDX) (Figure 7).

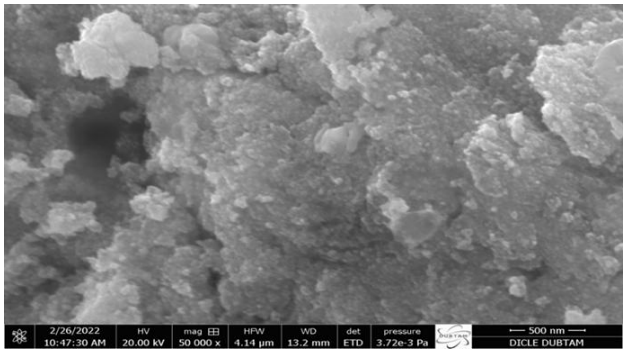

Figure 5. SEM images of biosynthesized OB-AuNPs

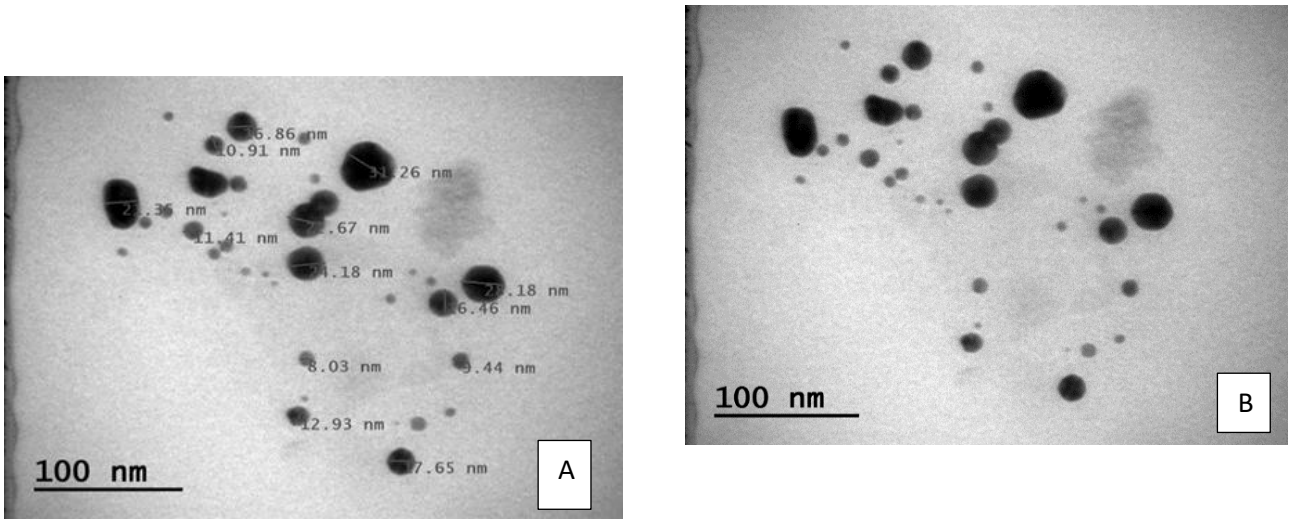

Figure 6. TEM images of biosynthesized OB-AuNPs (a, b)

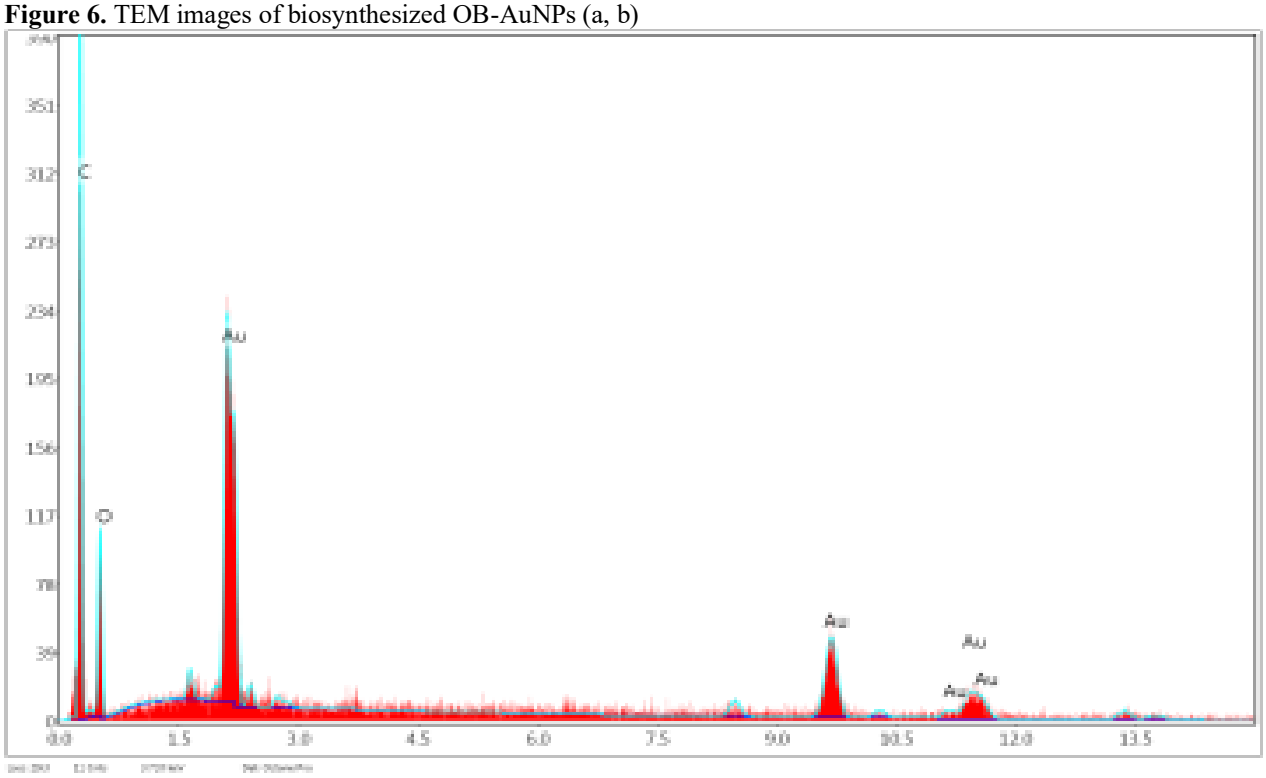

Figure 7. SEM-EDX spectrum of biosynthesized OB-AuNPs

AFM Analysis Results

AFM makes it possible to take measurements without the need for electrically conducting surfaces. With its high vertical image resolution, this Scanning Probe Microscope (SPM) instrument can scan the surface of a sample the size of a nanoparticle to acquire images and conduct surface interaction properties, friction, wear, corrosion, coating detection, electrical charge, absorption, and distribution research in the nanomaterial's structure, as well as size and shape research. Hydrophilic and magnetic characteristics can also be measured with it. OB-AuNPs' topological characteristics as determined by atomic force microscopy (AFM) were given in Figure 8.

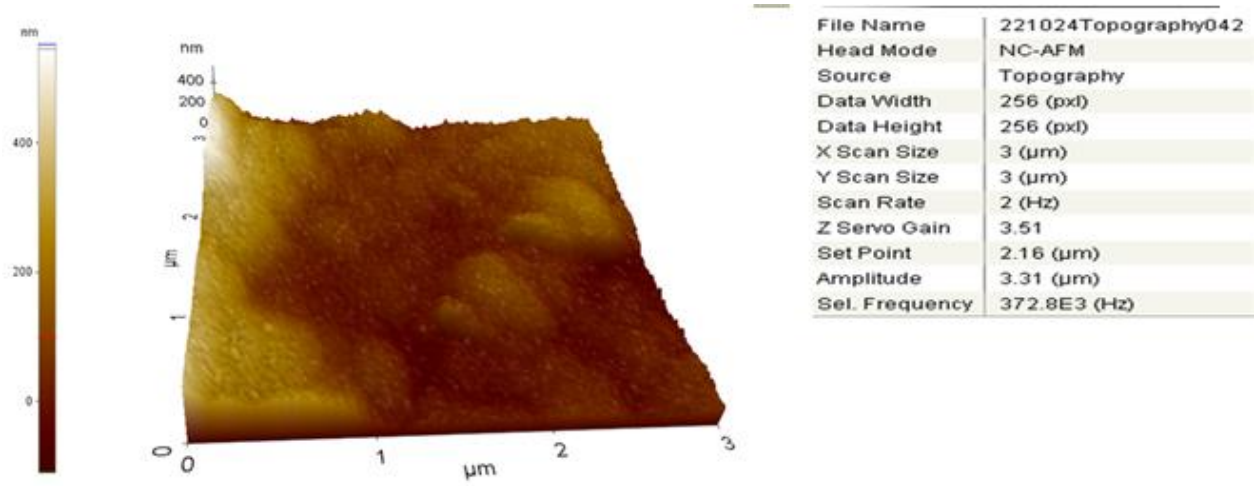

Figure 8. Atomic force microscopy (AFM) image of OB-AUNPs

Thermogravimetric (TGA) and Differential Thermal (DTA) Analysis Results of OB-derived Au NPs

TGA-DTA analysis was used to determine the degradation temperatures of gold nanoparticles produced using OB leaf extract. The TGA and DTA processes are used together. While TGA measures weight changes (water loss and organic matter removal) that take place inside the material, the DTA instrument measures temperature changes caused by exothermic/endothermic processes. This combined approach provides a comprehensive understanding of the thermal stability and behavior of the nanoparticles under varying temperatures. By analyzing the data obtained from both TGA and DTA, researchers can better assess the effectiveness of the synthesis method and the potential applications of the gold nanoparticles. By accurately calculating the melting, boiling, and decomposition points, DTA offers information regarding crystallization and phase transitions. The stability of the produced gold nanoparticles and their breakdown temperature were ascertained by TGA and DTA analysis (Figure 9).

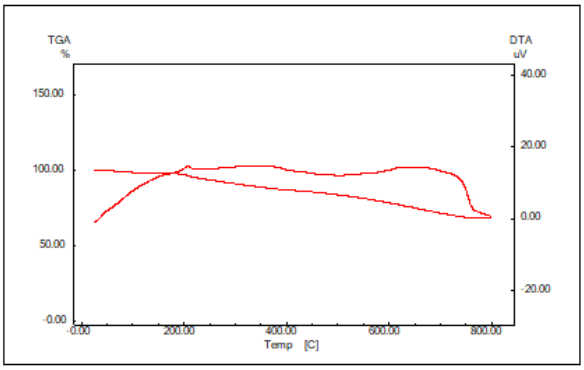

Figure 9. TGA-DTA analysis result of biosynthesized OB-AuNPs.

Zeta Potential and Distribution Analysis of OB-Au NPs

The Zeta potential and zetasizer were used to measure the surface charges and size distributions of AuNPs made from leaf extract. The electric charge on the surface of the

substance that is surrounded by the environment is known as the zeta potential. Adhesion and aggregation are inhibited by a large negative value of the zeta potential. This shows that the AuNP colloid is stable. However, because of their much lower negative charge, nanoparticles are able to enter the cell more readily (28). It was discovered that the biosynthesized AuNPs had a zeta potential of -17 mV (Figure 10). The AuNPs exhibiting monodispersity had an average zeta size of 166.2 (d.nm) according to the Zetasizer measurements (Figure 11).

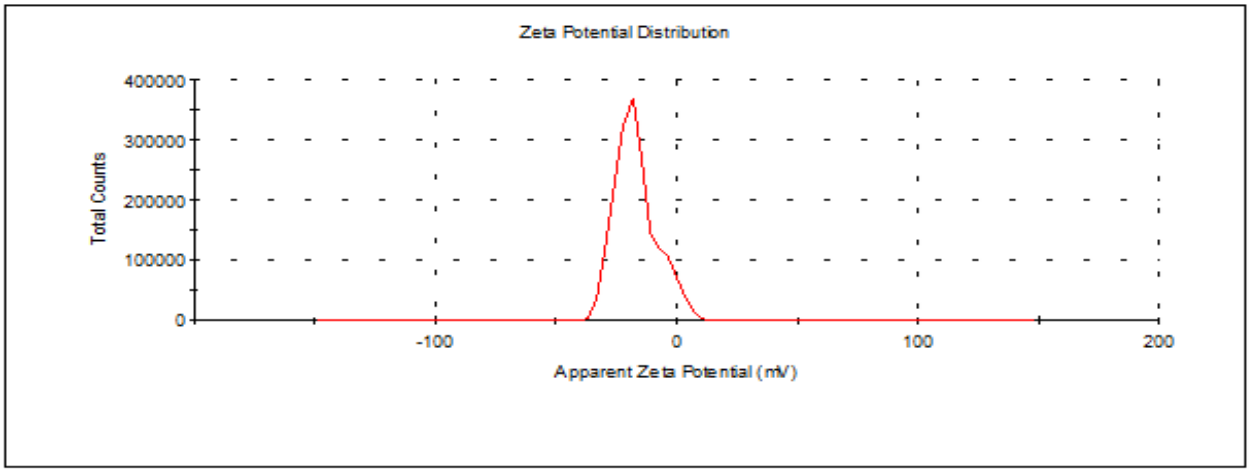

Figure 10. Zeta potential analysis of biogenic OB-AUNPs

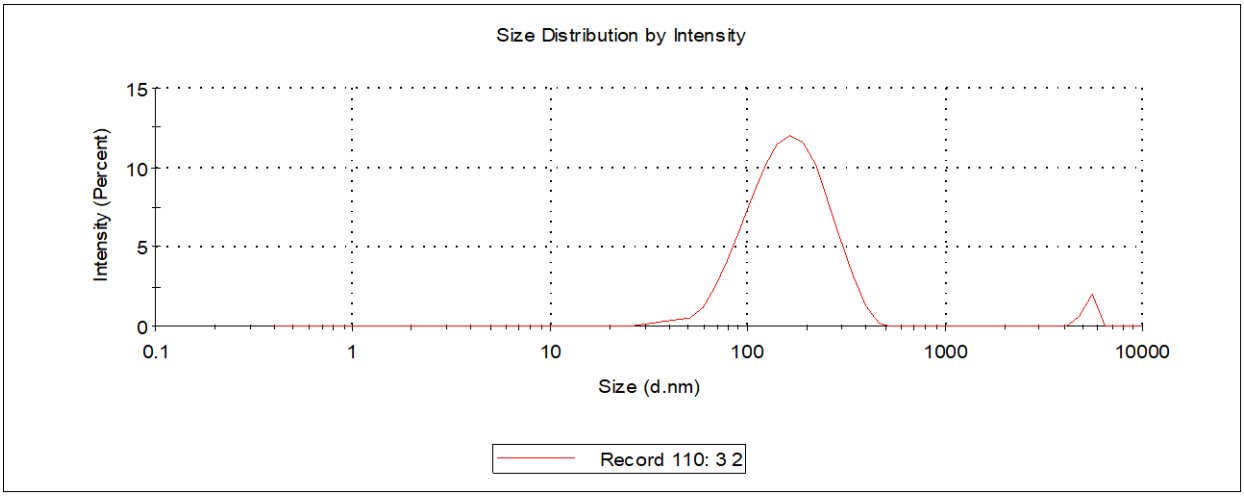

Figure 11. Zeta distribution analysis of biogenic OB-AUNPs

Antimicrobial Assay Results

The antimicrobial activity of biogenic OB-Au nanoparticles, which were created using an aqueous extract of OB leaves, was the main focus of this study. The study employed the minimum inhibitory concentration approach to assess antimicrobial activity against a variety of bacterial (gram positive *S. aureus*, gram negative *E. coli*) and yeast (*C. albicans*) strains. Throughout the experiment, fluconazole (128 µg/mL), colistin (128 µg/mL), and vancomycin

(128 µg/mL), served as standard. Table 1 demonstrates the strong antimicrobial activity of OB-AuNPs against Gram-positive and Gram-negative bacteria, as well as yeast. The antibacterial efficacy of gold nanoparticles is influenced by multiple factors, including zeta potential, particle size and shape, colloidal stability, pH, temperature, concentration, and the specific microbial strains tested.

Table 1. MIC value (µg/mL) of biogenic OB-AuNPs on pathogenic microorganisms

Microorganisms	OB-AuNPs	$AuCl_4.3H_2O$	Antibiotics*
S. aureus ATCC 29213	1. 40	2.65	2
E. coli ATCC25922	0.375	0.66	2
C. albicans	0.075	0.66	2

* *E. coli*, *S. aureus* and *C. albicans* were treated with colistin, vancomycin, and fluconazole antibiotics, respectively.

DISCUSSION

OB, among the Ocimum species, holds significant economic value due to its abundant volatile oil content and is extensively utilized in the spice, food, cosmetics, fragrance, and pharmaceutical sectors (29). The total phenolic content in green and purple varieties of OB is believed to be influenced by color variation, as well as species differences, climate, and cultivation conditions (30). Purple varieties of basil hold a key position in the food business due to their anthocyanin content, a crucial class of flavonoids that represent a substantial portion of plant secondary metabolites. The distinctive purple hue and the lack of estragole in its oil are noteworthy attributes for study subjects and economic viability. Consequently, the cultivation of OB is on the rise (31). The antibacterial efficacy of basil is influenced by factors such as its origin and oil composition; for instance, the effectiveness of French basil oil differs from that of Indian and Niazbo basil oils against *S. aureus*. French basil is ineffective, whereas Indian-niazbo basil is effective (32). The basil plant, comprising oil, protein, sugar, and water, occupies a role in the food chain due to its mineral content, including magnesium, potassium, phosphorus, iron, zinc, and calcium, and is also abundant in antibacterial compounds. It has been documented that it possesses anti-inflammatory, antioxidant, hypolipidemic, insecticidal, pharmacological, hypoglycemic, cardiac stimulant, anthelmintic, and wound-healing properties applicable in the treatment of cancer and ulcers resistant to bacterial, viral, and fungal infections (33).

The aqueous extract derived from OB leaves, noted for the aforementioned qualities, was utilized in the production of gold nanoparticles. The presence of stable gold nanoparticles produced through biosynthesis was validated using multiple spectroscopic techniques.

The UV-VIS spectrophotometer facilitates analytical analyses (both qualitative and quantitative) of colored complexes or

compounds within the wavelength range of 0.3-0.8 micrometers. It enables the examination of reaction kinetics, the calculation of equilibrium constants, the elucidation of molecular structures and stereochemical properties, and the identification of atoms and molecules. This includes the determination of anions that are undetectable by alternative instruments, the measurement of molecules or inorganic ions and complexes in solution, the assessment of purity levels, and the absorption of electromagnetic radiation by molecules or atoms, among other applications. The reduction of gold salt occurs through potent reducing agents, converting Au3+ ions to Au°, while surface plasmon resonance arises from the collective emission of free conduction electrons in gold solutions, influenced by the varying shape and size of the gold salt (10). In this context, UV-Vis spectroscopy, a crucial technique for detecting the formation and stability of AuNPs in aqueous solutions through colorimetric changes, was employed to assess the synthesis of AuNPs using basil (OB) plant extract. The maximum absorbance band color change of AuNPs, indicative of particle presence in the synthesis medium, was evaluated through UV-Vis readings. It was found that the color shift of AuNPs on the plasma surface caused a specific peak to appear at 532.59 nm in the UV-Vis spectrum. The synthesis accuracy is shown by studies that found particular peaks for AuNPs in the 525–540 nm range (10,34). These findings underscore the importance of precise control over the synthesis parameters to ensure consistent optical properties of AuNPs. Furthermore, the reproducibility of these peaks across different studies highlights the reliability of the synthesis techniques employed in the research. The study of the FT-IR results for the extract from OB leaves and its FT-IR spectrum after reacting with gold salt shows that the changes in frequency of the functional groups involved in the reduction are due to the vibrations of the O-H functional group at the 3347 cm^{-1} peak. The functional groups at 1634 cm^{-1} are linked to the I Amide band (C=C and C=N), while the peak at 2110 cm^{-1} might relate to the N=C or C=C functional groups. The functional groups at 1634 cm^{-1} are associated with the I Amide band (C=C and C=N), whereas the peak at 2110 cm^{-1} may correspond to the N=C or C=C functional groups. The changes in the frequencies indicate that the –OH (hydroxyl), N-H (amine), and C≡C (alkyne) groups are responsible for the decrease. This reduction shows that these functional groups are interacting strongly with their surroundings, which could affect how reactive and stable the compound is. Understanding these shifts in peak positions is crucial for elucidating the compound's chemical behavior and potential applications in various fields.

The X-Ray Diffraction method (XRD) is based on how X-rays bounce off materials, creating a pattern that shows the unique features of crystal structures, the distance between atoms, and how they are arranged in a crystal. X-rays are emitted from a cathode ray tube, filtered to provide monochromatic radiation, collected in a concentrated manner, and directed toward the sample. The diffracted X-rays are subsequently measured, analyzed, and quantified, and the XRD crystal structure is revealed. Diffraction serves to identify crystalline phases akin to a fingerprint. The crystal structure and purity of gold nanoparticles were verified using XRD analysis. Figure 4 illustrates the powder XRD patterns of nanocrystalline AuNPs. The diffraction peaks and planes for AuNPs, such as (111), (200), (220), and (311), match the face-centered cubic structure. The unique peak values corresponded well with the reference data (JCPDS card no. 0784 for Au) (35). The high-resolution and robust XRD pattern demonstrated the synthesis of crystalline AuNPs through the reduction of Au+ ions using an extract from OB leaves. The analysis of the XRD data revealed that the average nanoparticle size was determined to be 40.39 nm, as per the Debye-Scherrer equation. This size is consistent with the expected dimensions for effective catalytic activity and biocompatibility in various applications. Furthermore, the successful synthesis of these gold nanoparticles underscores the potential of using plant extracts as eco-friendly alternatives in nanomaterial production.

In a scanning electron microscope, electrons interact with atoms in the sample and produce signals that reveal the sample's topography and composition. This work used SEM to analyze the morphological structures of gold nanoparticles that were generated. A two-dimensional and detailed sample image is obtained with TEM. Imaging of the sample's surface and fine structures, morphological research, and structure-function interpretation are possible. TEM examination shows how a substance's physical characteristics and microstructures generate a common feature or features. TEM investigation of gold nanoparticles is conducted by capturing images at very low nanometers, evaluating their size, and determining their average size. It also helps determine the cell membrane transit of produced metallic nanoparticles in biological applications. Transmission Electron Microscopy analyzes samples using high-voltage electron beams. SEM and EDX micrographs provide further data regarding the scanned region's chemical and elemental compositions. Nano-characterization uses SEM and EDX to determine particle sizes and elemental composition. In electron dispersive X-ray (EDX) analysis (Figure 7), the sample's elemental compositions suggest AuNPs with strong gold peaks. In addition, the scanned spots determine the metalloid composition

percentage. Quantitative examination of the produced gold nanoparticles follows. The evaluation of the acquired results revealed that the gold nanoparticles were spherical. The SEM-EDX analysis of the AuNPs' energy distribution spectra revealed that the gold particles were roughly 50 nm in size and that the majority of the elemental composition was that of gold nanoparticles. The functional groups of phytochemicals around the reduction-formed nanoparticles are responsible for the occurrence of peaks like carbon and oxygen next to these strong peaks. The dimensions of the produced nanomaterial were assessed using TEM metrics. According to the TEM pictures of the produced AuNP-OB, the synthesized AuNPs have an average size of 17.79 nm and range in size from 8.03 to 31.26 nm (Figure 6a,b). Because of their functional groups and surface charges, the AuNPs produced via green synthesis are nanosized and arranged in small groups that are not in direct touch with one another, according to micrographs (10).

The AFM results show that the average particle size of AuNPs is between 0-100 nm as seen in Figure 8. The surface morphology of AuNPs, SEM and TEM images (Figure 5 and Figure 6a,b) and particle distribution density analysis (Figure 7) confirm the existence of AuNPs obtained by synthesis in nano-sized and non-contacting clusters. This shows that AuNPs are stable and do not agglomerate due to their negative surface charge. In addition, TEM images indicate that gold particles are predominantly spherical and hexagonal in size. Many researchers have also reported spherical AuNPs in their studies (36).

The gold nanoparticles produced biologically were examined using TGADTA data from 20 to 800 °C at a heating rate of 10 °C per minute in a nitrogen environment with a flow rate of 20 mL per minute. The TGA-DTA curve illustrates the mass reduction resulting from thermal deformation. Figure 9 illustrates that the mass loss within the temperature range of 0-200 °C is attributable to moisture, but the mass losses occurring between 200-800 °C are a result of the plant extract. The nanomaterial remains stable at elevated temperatures, with the mass loss amounting to 25 percent. Research has documented the stable architectures of nanoparticles at elevated temperatures, specifically in research with AuNPs derived from *Acacia auriculiformis* (37) and *Artemisia absinthium* (38).

The antimicrobial mechanism of nanoparticles frequently seeks to examine the interactions between nanoparticles and the bacterial cell membrane, as well as the parameters that allow the bacteria to sustain its viability. Research indicates that substantial quantities of particles are generated, and nanoparticles with elevated surface area exhibit significant activity at minimal concentrations (39). Metal particles attach to the cell membrane via nanoparticles, utilizing electrical forces and chemical bonds to

form a composite structure. In response to the adherence of the metal particle, the cell undergoes dissolution by oxidation, resulting in the combination of atoms and ions to form bigger particles. The interactions of metal nanoparticles vary between living and deceased cells. Table 1 illustrates the inhibitory effect of biosynthesized OB-AuNPs on human pathogens. The inhibitory impact of AuNPs is evidently superior to that of $HAuCl_4.3H_2O$ and antibiotics, even at minimal dosages. The most potent action of OB-AuNPs was observed against *C. albicans* at a concentration of 0.075 µg/mL. The MIC values (µg/mL) of the synthesized AuNPs for *S. aureus* and *E. coli* were established as 1.40 and 0.375, respectively. The current investigation reveals the presence of AuNPs at around 8 nm (Figure 6a). Agnihotri et al. (2014) reported that when nanoparticles smaller than 10 nm get even smaller, they can enter cells more easily, which makes AuNPs more effective at fighting bacteria (40). The antibacterial efficacy of AuNPs was assessed using the microdilution method, wherein the Minimum Inhibitory Concentration (MIC) values were established for the gram-positive *S. aureus*, gram-negative *E. coli*, and the fungus *C. albicans*. Consequently, it was concluded that OB-AuNPs exhibited superior antibacterial efficacy relative to commercial antibiotics at low doses. This enhanced cellular uptake could lead to improved therapeutic outcomes, particularly in treating infections caused by resistant bacterial strains. Future studies should focus on the mechanisms of interaction between these nanoparticles and bacterial cells to further elucidate their potential applications in antimicrobial therapy.

CONCLUSION

This research is the first investigation into the biological applications of gold nanoparticles synthesized from the aqueous extract of OB leaves. The exceptional characteristics of AuNPs render these compounds widely sought after, presenting significant application prospects in biomedicine. This research focused on an easy, quick, cheap, and environmentally friendly way to make OB-AuNPs using the water extract from OB leaves. The unique characteristics of OB-AuNPs were examined using methods like UV-Vis, zeta potential, XRD, SEM, EDX, TEM, AFM, and TGA-DTA. OB-AuNPs had a stable structure, absorbed the lightest at 532.59 nm, had a one-dimensional shape, and had a surface charge of (-)17 mV. The TEM analysis revealed that the nanoparticles were spherical, measuring between 8 and 31 nm in size. The crystalline characteristics of AuNPs were ascertained using XRD analysis. The EDX spectra showed a strong peak between 2–2.5 keV, indicating that gold is a major part of the gold nanoparticles. The nanoparticles were uniformly distributed throughout the sample, as evidenced in the solid phase. The aqueous

extract of OB appears to inhibit the aggregation of AuNPs. The microdilution technique was employed to assess the impact of OB-AuNPs on pathogenic microorganisms to ascertain their potential as a therapeutic agent. OB-AuNPs showed the ability to kill bacteria and fungi, significantly stopping their growth at concentrations between 0.075 and 1.40 g/mL. Improving or changing the features of the OB-AuNPs created will greatly help research on antibiotic resistance in bacterial infections. This enhancement could lead to the development of more effective treatments that can overcome the challenges posed by resistant strains. Additionally, further investigation into the mechanisms of action of OB-AuNPs could provide valuable insights into their role in combating microbial infections.

Acknowledgments: The authors are thankful to Mardin Artuklu University, for providing all necessary research facilities to carry out this research.

Ethics Committee Approval: Ethics committee approval is not required as there is no human or animal research.

Peer-review: Externally peer-reviewed

Author Contributions: Concept: HKO, MKÇ, YEİ, Design: HKO, MKÇ, YEİ, Data Collection and Processing: HKO, MKÇ, YEİ, Analysis and Interpretation: HKO, MKÇ, YEİ, Writing: HKO, MKÇ, YEİ

Conflict of Interest: The authors declared no conflict of interest.

Financial Disclosure: The authors declared that this study has not received no financial support.

REFERENCES

1. Kumar A, Jayeoye TJ, Mohite P, Singh S, Rajput T, Munde S, et al. Sustainable and consumer-centric nanotechnology-based materials: An update on the multifaceted applications, risks and tremendous opportunities. Nano-Structures & Nano-Objects, 2024; 38: 101148.
2. Forooque F, Mughees MM, Wasi M, Khan MS. Green sustainable nanoparticles as a drug delivery system—an updated review. Sustainable Nanomaterials: Synthesis and Environmental Applications. 2024; 171-201.
3. Petrovic S, Bita B, Barbinta-Patrascu ME. Nanoformulations in pharmaceutical and biomedical applications: green perspectives. International Journal of Molecular Sciences. 2024; 25(11): 5842.
4. Ertaş E, Doğan S, Baran A, Baran M.F, Evcil M, Kurt B, et al. Preparation and characterization of silver-loaded magnetic activated carbon produced from *Crataegus*

monogyna for antimicrobial and antioxidant applications. ChemistrySelect. 2025; 10: e202405558.

5. Eftekhari A, Khalilov R, Kavetskyy T, Keskin C, Prasad R, Rosic GL. Biological/chemical-based metallic nanoparticles synthesis, characterization, and environmental applications. Frontiers in Chemistry. 2023; 11: 1191659.
6. Baran, M. F., Keskin, C., Baran, A., Hatipoğlu, A., Yildiztekin, M., Küçükaydin, et al. (2023a). Green synthesis of silver nanoparticles from *Allium cepa* L. Peel extract, their antioxidant, antipathogenic, and anticholinesterase activity. Molecules, 28(5), 2310.
7. Wozniak A, Malankowska A, Nowaczyk G, Grześkowiak B, Tuśnio K, Slomski R, et al. Size and shape-dependent cytotoxicity profile of gold nanoparticles for biomedical applications. Journal of Materials Science: Materials in Medicine. 2017; 28: 92. https://doi.org/10.1007/s10856-017-5902-y.
8. Hazbar AM, Mohammed Noori Jassim A, Taha Mohammed M. Green synthesis of gold nanoparticles using *Eruca sativa* plant extracts. Journal of Nanostructures, 2025; 15(1): 158-167.
9. Brust M, Bethell D, Kiely CJ, Schiffrin DJ. Self-Assembled gold nanoparticle thin films with nonmetalic optical and electronic properties", Langmuir. 1998; 14: 5425-5429.
10. Keskin C, Baran A, Baran MF, Hatipoğlu A, Adican MT, Atalar MN, et al. Green synthesis, characterization of gold nanomaterials using *Gundelia tournefortii* leaf extract, and determination of their nanomedicinal (antibacterial, antifungal, and cytotoxic) potential. Journal of Nanomaterials. 2022; 2022: 7211066. https://doi.org/10.1155/2022/7211066.
11. Aminabad NS, Farshbaf M, Akbarzadeh A. Recent advances of gold nanoparticles in biomedical applications: State of the art. Cell Biochemistry and Biophysics. 2019; 77(2): 123-137.
12. Mehra V, Kumar S, Tamang AM, Chandraker SK. Green synthesis of gold nanoparticles (AuNPs) by using plant extract and their biological application: A review. BioNanoScience. 2025; 15(1): 1-20.
13. Hammad SE, El-Rouby MN, Abdel-Aziz MM, El-Sayyad GS, Elshikh HH. Endophytic fungi–assisted biomass synthesis of gold, and zinc oxide nanoparticles for increasing antibacterial, and anticancer activities. Biomass Conversion and Biorefinery. 2025; 15(2): 2285-2302.
14. Aamir M, Hassan S, Khan AH, Ibrar M, Sarwar S, Mahmood K. et al., Spirulina-mediated biosynthesis of gold nanoparticles:

an interdisciplinary study on antimicrobial, antioxidant, and anticancer properties. Journal of Sol-Gel Science and Technology. 2025; 1-13.

15. Nunes A, Rilievo G, Magro M, Maraschin M, Vianello F, Lima GPP. Biotechnological applications of biogenic nanomaterials from red seaweed: A systematic review (2014–2024). International Journal of Molecular Sciences. 2025; 26(9): 4275.

16. Ojha S, Khan A, Sahoo CR, Mohapatra RK, Tripathi DK, Mukherjee M, et al. A Review on Biosynthesis of Nanoparticles via Microalgal Technology and Their Biomedical Applications. BioNanoScience. 2025; 15(2): 1-22.

17. Barsola B, Saklani S, Pathania D, Kumari P, Sonu S, Rustagi S, et al. Exploring bio-nanomaterials as antibiotic allies to combat antimicrobial resistance. Biofabrication. 2024; 16(4): 042007.

18. Zambonino MC, Quizhpe EM, Mouheb L, Rahman A, Agathos SN, Dahoumane SA. Biogenic selenium nanoparticles in biomedical sciences: properties, current trends, novel opportunities and emerging challenges in theranostic nanomedicine. Nanomaterials. 2023; 13(3): 424.

19. Chaturvedi VK, Sharma B, Tripathi AD, Yadav DP, Singh KR, Singh J, et al. Biosynthesized nanoparticles: a novel approach for cancer therapeutics. Frontiers in Medical Technology, 2023; 5: 1236107.

20. Baydar H. Tıbbi ve Aromatik Bitkiler Bilimi ve Teknolojisi (Genişletilmiş 4. Baskı), Süleyman Demirel Üniversitesi. 2013; Yayın No: 51 (ISBN: 975-7929-79-4).

21. Shahivand M, Mir Drikvand R, Gomarian M, Samiei K. Evaluation of expression stability of some reference genes in green and red cultivars of sweet basil (*Ocimum basilicum* L.) under abiotic stresses. Crop Biotechnology. 2021; 10(4): 67-78.

22. Shikha D, Kashyap P. *Ocimum* species. Harvesting Food From Weeds. 2023; 183-215.

23. Divani S, Paknejad F, Ghafourian H, Alavifazel M, Ardakani MR. Feasibility study on reducing lead and cadmium absorption in sweet basil (*Ocimum basilicum* L.) with using active carbon. Journal of Crop Nutrition Science. 2017; 3(1): 25-36.

24. Keskin C, Aslan S, Baran MF, Baran A, Eftekhari A, Adıcan MT, et al. Green synthesis and characterization of silver nanoparticles using *Anchusa officinalis*: antimicrobial and cytotoxic potential. International Journal of Nanomedicine. 2025; 2025: 4481-4502.

25. Kumar R, Ghosh A, Patra CR, Mukherjee P, Sastry M. Gold Nanoparticles Formed within. Nanotechnology in Catalysis. 2004; 1(2): 1-111.

26. Hong S, Li X. Optimal size of gold nanoparticles for surface-enhanced Raman spectroscopy under different conditions. Journal of Nanomaterials. 2023; 2013(1): 790323.

27. Mapala K, Pattabi M. *Mimosa pudica* flower extract mediated green synthesis of gold nanoparticles. NanoWorld Journal. 2017; 3(2): 44-50.

28. Egata DF. Benefit and use of sweet basil (*Ocimum basilicum* L.) in Ethiopia: A review. Journal of Nutrition and Food Processing. 2021; 4(5): 57-59.

29. Mccance KR, Flanigan PM, Quick MM, Niemeyer ED. Influence of plant maturity on anthocyanin concentrations, phenolic composition, and antioxidant properties of 3 purple basil (*Ocimum basilicum* L.) cultivars. Journal of Food Composition and Analysis. 2016; 53: 30–39.

30. Simon JE, Morales MR, Phippen WB, Vieira RF, Hao Z. A source of aroma compounds and a popular culinary and ornamental herb. In J. Janick (Ed.), Perspectives on new crops and new uses, Alexandria, VA: ASHS Press, 1999; 499–505.

31. Hiltenun R, Holm Y. Essential oil of Ocimum. In R. Hiltunen & Y. Holm (Eds.). Basil: The genus *Ocimum* (Vol. 10).: Harwood Academic Publishers, Amsterdam, 1999; 13–135.

32. Marwat SK, Rehman FU, Khan MS, Ghulam S, Anwar N, Mustafa G, et al. Phytochemical constituents and pharmacological activities of sweet basil *Ocimum basilicum* L. (Lamiaceae). Asian Journal of Chemistry. 2011; 23(9): 37733782.

33. Duan J, He D, Wang W, Liu Y, Wu H, Wang Y, et al. The fabrication of nanochain structure of gold nanoparticles and its application in ractopamine sensing. Talanta, 2013; 115: 992-998.

34. Ahmady IM, Parambath JB, Elsheikh EA, Kim G, Han C, Pérez-García, et al. Bacterial synthesis of anisotropic gold nanoparticles. Applied Microbiology and Biotechnology, 2025; 109(1): 62.

35. Baran MF, Keskin C, Baran A, Eftekhari A, Omarova S, Khalilov R, et al. The investigation of the chemical composition and applicability of gold nanoparticles synthesized with *Amygdalus communis* (almond) leaf aqueous extract as antimicrobial and anticancer agents. Molecules. 2023b; 28(6): 2428.

36. Hamelian M, Varmira K, Veisi H. Green synthesis and characterizations of gold nanoparticles using Thyme and survey cytotoxic effect, antibacterial and antioxidant potential. Journal of Photochemistry and Photobiology B: Biology, 2018; 184: 71-79.

37. Parveen M, Kumar A, Khan MS, Rehman R, Furkan M, Khan RH, et al. Comparative study of biogenically synthesized silver and gold nanoparticles of *Acacia auriculiformis* leaves and their efficacy against Alzheimer's and Parkinson's disease. International Journal of Biological Macromolecules. 2022; 203: 292-301.

38. Baran MF, Keskin C, Atalar MN, Baran A. Environmentally friendly rapid synthesis of gold nanoparticles from *Artemisia absinthium* plant extract and application of antimicrobial activities. Journal of the Institute of Science and Technology, 2021,11. 365-375.

39. Sundaresan P, Krishnapandi A, Chen SM. Design and investigation of *Ytterbium tungstate* nanoparticles: An efficient catalyst for the sensitive and selective electrochemical detection of antipsychotic drug chlorpromazine. Journal of the Taiwan Institute of Chemical Engineers. 2019; 96: 509-519.

40. Agnihotri S, Mukherji S, Mukherji S. Size-controlled silver nanoparticles synthesized over the range 5–100 nm using the same protocol and their antibacterial efficacy. Rsc Advances, 2014; 4(8): 3974-3983.